nature communications

Article

https://doi.org/10.1038/s41467-025-58095-9

A wearable repetitive transcranial magnetic stimulation device

Received: 3 September 2024

Accepted: 6 March 2025

Published online: 19 March 2025

Check for updates

Zihui Qi[1,2,3,6], Hao Liu[1,2,3,4,6], Fang Jin[1,2], Yihang Wang[1,2], Xuefeng Lu[1,2], Ling Liu[1,2], Zhengyi Yang[1,2,5], Lingzhong Fan[1,2], Ming Song[1,2,5], Nianming Zuo[1,2] & Tianzi Jiang[1,2,4,5]

Repetitive transcranial magnetic stimulation (rTMS) is widely used to treat various neuropsychiatric disorders and to explore the brain, but its considerable power consumption and large size limit its potential for broader utility, such as applications in free behaviors and in home and community settings. We addressed this challenge through lightweight magnetic core coil designs and high-power-density, high-voltage pulse driving techniques and successfully developed a battery-powered wearable rTMS device. The combined weight of the stimulator and coil is only 3 kg. The power consumption was reduced to 10% of commercial rTMS devices even though the stimulus intensity and repetition frequency are comparable. We demonstrated the effectiveness of this device during free walking, showing that neural activity associated with the legs can enhance the cortex excitability associated with the arms. This advancement allows for high-frequency rTMS modulation during free behaviors and enables convenient home and community rTMS treatments.

High-intensity transcranial electrical stimulation (TES) and repetitive transcranial magnetic stimulation (rTMS) are the two most commonly used non-invasive neuro-modulation techniques capable of eliciting supra-threshold neuronal responses in the human brain[1,2]. Due to its high stimulation intensity and noticeably reduced discomfort and side effects compared with high-intensity transcranial electrical stimulation[3,4], rTMS has found extensive applications in treating various neuropsychiatric disorders[5,6] as well as being a vital non-invasive tool in cognitive neuroscience research[7,8]. However, current rTMS devices are not suitable for portable or wearable applications due to their bulky size and considerable power consumption, on the order of a kilowatt[9,10]. Some of the results of these limitations are: Because of the inability to conduct rTMS during spontaneous and free behaviors in diverse real-world settings, our understanding of neural modulation in dynamic environments is limited[11–13], and walking investigations conducted on laboratory treadmills cannot fully replicate the real-life scenarios experienced by subjects[14]. In addition, the current inability to administer rTMS during neurorehabilitation training hampers the potential enhancement of neuroplasticity and rehabilitation outcomes[15,16]. Another result is that the prevalent hospital-based approach for rTMS treatment in neuropsychiatric disorders such as depression is cost-prohibitive, demanding trained medical staff for daily treatments over a month[5,17], making it challenging for patients to sustain regular work routines, and affecting treatment adherence and outcomes[18,19]. Hence, there is an urgent need for a portable or wearable rTMS device that can meet the demands of neuromodulation during free behaviors, rehabilitation training, and in home and community settings. The possibility of portable or wearable rTMS devices is attractive for the treatment of many pathologies[20].

Several research teams and companies are working on developing portable TMS devices, but progress has been quite slow due to power consumption and volume reduction challenges. Initial progress has

[1]Beijing Key Laboratory of Brainnetome and Brain-Computer Interface, Institute of Automation, Chinese Academy of Sciences, Beijing, China. [2]Brainnetome Center, Institute of Automation, Chinese Academy of Sciences, Beijing, China. [3]University of Chinese Academy of Sciences, Beijing, China. [4]School of Artificial Intelligence, University of Chinese Academy of Sciences, Beijing, China. [5]Xiaoxiang Institute for Brain Health and Yongzhou Central Hospital, Yongzhou, Hunan Province, China. [6]These authors contributed equally: Zihui Qi, Hao Liu. e-mail: jiangtz@nlpr.ia.ac.cn

been made with portable TMS devices that provide relatively low-intensity subthreshold magnetic stimulation[21,22]. Commercial low-intensity subthreshold magnetic stimulation devices, such as NeoRhythm (https://omnipemf.com/), which can only output magnetic pulses at 0.0025 Tesla, are currently available. However, these devices cannot directly trigger action potentials and fall far short of the stimulation intensity required for FDA-approved TMS (greater than 1 Tesla). Epstein developed a 3 kg battery-powered portable single-pulse TMS. Charging required 25 s on average, reaching maximum power in 45 s[23]. eNeura's SpringTMS (now named sTMS mini) is the only FDA-approved portable TMS for the treatment of acute migraines. It weighs approximately 1.7 kg and delivers 2 pulses per stimulation cycle[24]. While the aforementioned devices are battery-powered portable TMS systems, they are primarily designed for single-pulse TMS (sTMS) and cannot effectively accommodate rTMS applications such as 1 Hz, 10 Hz, or intermittent theta burst stimulation (iTBS). REMED developed a small household rTMS device (TAMAS) with dimensions of 430 × 270 × 89 mm and a weight of 4.5 kg. However, the coil in this system tends to overheat during rTMS treatments, requiring coil replacement every 10 min. Additionally, the system relies on AC power, which makes it impractical for ambulatory or wearable use[25]. Abbasi et al. designed miniaturized rTMS head coils with a diameter of 38 mm and a weight of 12.6 g[26]. Their prototype has reduced the size and weight to approximately 1/10th of a full-scale clinical system[27], but the maximum magnetic flux density achieved is relatively low (0.54 Tesla), and this system has not been tested for supra-threshold neuronal responses in the human brain. All the aforementioned devices and their specifications are listed in Table S1. To summarize, no battery-powered portable or wearable supra-threshold rTMS (operating at 10 Hz or 50 Hz) device is currently available.

To address these issues, we developed a battery-powered wearable rTMS device, rTMS-tiny, by applying lightweight magnetic core coil technology and high-power-density, high-voltage pulse driving techniques. The combined weight of the stimulator and coil is only 3 kg. The power consumption was reduced to 10% of commercial rTMS devices even though the stimulus intensity and repetition frequency are comparable to those of the commercial rTMS devices. Remarkably, rTMS-tiny is able to achieve repetition frequency and stimulus intensity that match the Super Rapid² Plus commercial rTMS device from Magstim. This is the first battery-powered, wearable supra-threshold rTMS device, meeting the demand for on-the-go rTMS neuromodulation.

Results

A super compact battery-powered magnetic stimulator and a lightweight magnetic core coil enable wearable rTMS

rTMS-tiny consists of a battery-powered, super-compact magnetic stimulator and a lightweight magnetic core figure-8 coil (Fig. 1a). The magnetic core coil weighs 1.7 kg, and has an average coil diameter of 63 mm and an outer diameter of 78 mm. The magnetic stimulator measures 17 cm × 14 cm × 6 cm and weighs 1.3 kg. The magnetic stimulator connects to and drives the magnetic core coil via a 1.5-meter cable, generating sinusoidal biphasic pulses with a pulse width of 348 μs and a maximum magnetic flux density of 1.2 Tesla. It can achieve a repetition output frequency of up to 100 Hz (Fig. 1b) with a maximum intensity of 55% of the maximum stimulator output (MSO), meeting the requirements of the majority of rTMS applications. Under the natural cooling of room temperature at 25 °C, the coil temperature measured only 36.1 °C after 3000 pulses of 10 Hz rTMS at 70% MSO. rTMS-tiny is powered by an 18 V 2200 mAh lithium battery, and can deliver 8200 pulses at 70% MSO for 10 Hz of rTMS. To enable it to be worn, the magnetic core coil is secured to the head using an elastic band that wraps around the chin, and the portion of the coil that contacts the head is padded with foam. This configuration increases the contact area between the coil and the scalp, reduces pressure on the scalp, and enhances stability. The positioning of the coil is assisted by a 10–20 EEG electroencephalogram positioning cap, with the left primary motor cortex (M1) at C3. The rTMS-tiny stimulator can be easily held in one hand and operated with the other (Fig. 1c) and can also be conveniently worn on the body (Fig. 1d). This allows for neuromodulation with rTMS to be conducted during free behaviors, in space-constrained conditions and in home and community settings, significantly expanding the application scenarios for rTMS.

The bent double-T magnetic core coil achieves ultra-low power consumption without adding weight

Reducing power consumption is a prerequisite for achieving a wearable rTMS. Abbasi et al. developed a compact (38 mm in diameter), lightweight (12.6 g) figure-8 coil capable of inducing an electric field of 87 V/m at a depth of 1.5 cm. While small coils are advantageous due to their light weight and low power consumption, they sacrifice penetrability and stimulation intensity[26,27]. Methods that reduce power consumption while maintaining stimulation intensity include the use of minimal energy coils, double-cone coils, and magnetic core coils[28]. Compared with traditional figure-8 coils, minimal energy coils can achieve a 41% energy saving as a result of the optimization of the winding pattern[29]. Double-cone coils can save up to 53% of the energy[30], albeit at the expense of focusing[31]. Magnetic core coils can achieve a remarkable 73% energy savings[32], and are currently the most effective energy-saving method. Compared with the hollow condition (Fig. S1a), the magnetic flux density B of magnetic core coils (Fig. S1b) can be doubled at the same driving current. But one challenging drawback of magnetic core coils is their significant weight increment. Existing magnetic core coil designs typically employ flat plate cores[33] or C-shaped cores[32] (Fig. S1c, d). To prevent magnetic core saturation[34], the core's cross-sectional area needs to be sufficiently large, leading to significant core weight. For instance, the dimensions of the backplate core in Yamamoto and colleagues[35] are 22 cm × 12.2 cm × 1 cm with a core weight of approximately 2.1 kg. Epstein and Davey[32] utilized a smaller C-shaped core, with dimensions approximating a cylinder with a diameter of 10 cm and a height of 5 cm and weighing over 1.5 kg. Reducing the weight of the magnetic core coil is essential for meeting the requirements of wearable rTMS devices. Given the limitations in performance of the existing conductor and magnet materials, reducing the diameter of the magnetic core coil effectively reduces weight. However, as the coil diameter decreases, the magnetic field penetration capability weakens, although the focus can be enhanced[36,37]. Conversely, by bending the coil wings toward the brain, double-cone coils increase coupling with the brain and improve penetration depth but sacrifice focus[31].

We designed a bent double-T magnetic core figure-8 coil with an average coil diameter of 63 mm, T2-Bent-D63 (Fig. 2d) by combining and optimizing the magnetic core coil and the double-cone coil. This design reduces the weight and the required magnetic field energy by shrinking the coil diameter. It also enhances penetration by bending the coil, compensating for the weakness in penetration capability associated with a small-diameter coil while keeping the focal properties nearly unchanged. The T-shaped magnetic core consists of one small and one large thin cylinder connecting at their centers. The core weight is only 1.2 kg, making it suitable for wearable applications.

To find the optimal bending angle, we conducted electromagnetic field simulations using COMSOL Multiphysics software (Fig. 2a–i). The T2-Bent-D63 coil was configured with air-core 0° (no magnetic core and no bending) and with a magnetic core and bending angles of 0°, 10°, 20°, and 30°. The simulation results showed that the magnetic core increased the induced electric field strength from 61 V/m in the hollow state to 127 V/m (Fig. S2a–f). However, it still differed significantly from the 150 V/m of the Magstim D70 coil. Bending further enhanced the induced electric field strength, reaching a maximum value of 141 V/m when the bending angle was 30°. This was

https://doi.org/10.1038/s41467-025-58095-9

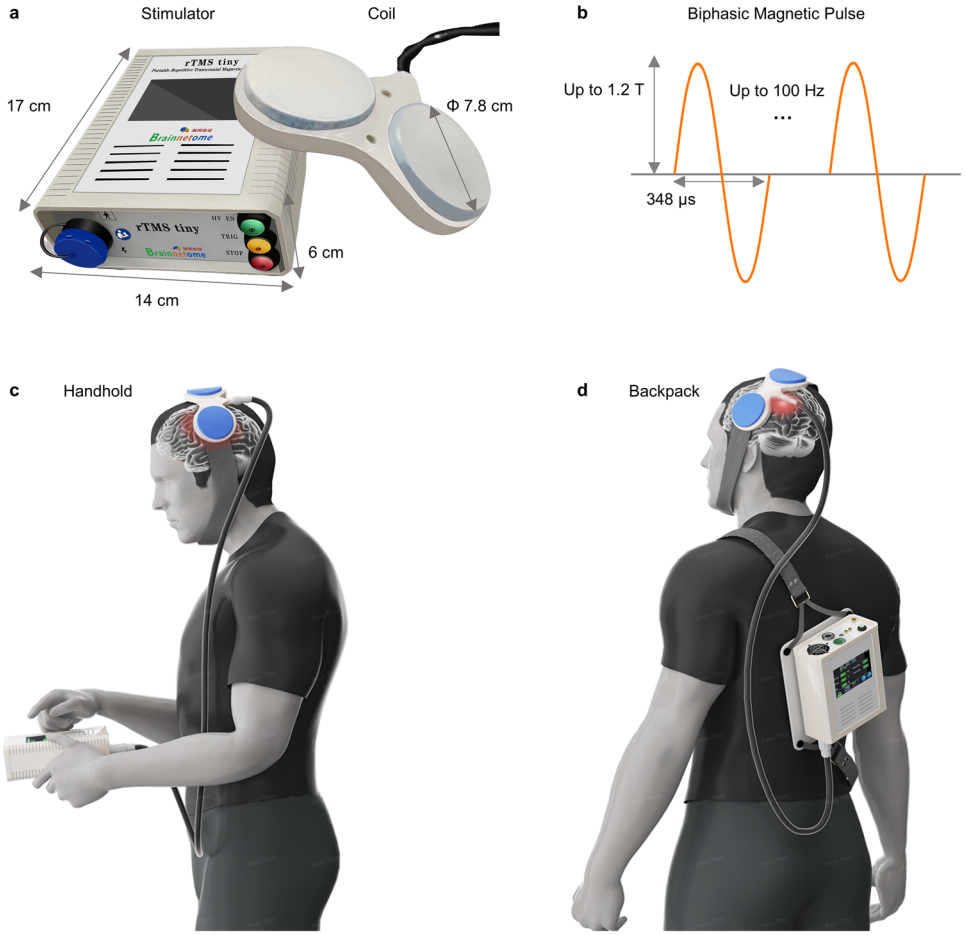

Fig. 1 | Comprehensive illustration of the wearable rTMS device. a rTMS-tiny consists of a magnetic stimulator and a magnetic core figure-8 coil. The magnetic core coil weighs 1.7 kg, with an outer diameter of 78 mm. The magnetic stimulator measures 17 cm × 14 cm × 6 cm and weighs 1.3 kg. These are connected by a 1.5-meter cable. **b** Output of sinusoidal biphasic magnetic pulse with a pulse width of 348 μs, a maximum magnetic flux intensity of 1.2 Tesla on the coil surface, and a maximum repetition frequency of 100 Hz. **c** Handheld operation with pulse control through a touchscreen interface. The magnetic core coil is secured to the head using an elastic band that wraps around the chin. The portion of the coil that contacts the head is padded with foam, increasing the contact area, reducing pressure on the scalp, and enhancing stability. **d** The device is worn on the body, with the stimulator secured across the back using a single or dual shoulder strap configuration, freeing the hands and enabling rTMS stimulation during free behaviors.

approximately 94% of the Magstim D70 coil (Fig. 2g) and had equivalent penetration capabilities (Fig. 2h) and slightly better spatial focus than the D70 coil (Fig. 2i). Again, this configuration met the requirements for a wearable rTMS device. Additionally, the magnetic core had been fully utilized, with the maximum magnetic flux intensity (B) approaching saturation (Fig. 2f). The electric field distributions in the scalp are shown in Fig. S3. The maximum electric field intensity in the scalp for the T2-Bent-D63 coil was 288 V/m, which is lower than the 323 V/m of the Magstim D70 coil and is, therefore, unlikely to cause greater injury or pain.

We wound the coil using rectangular litz wire with a filling factor of 50%, reducing the weight of the coil by half compared with flat copper wire. The coil's weight is only 263 g, and its alternating current (AC) resistance remains nearly constant between 100 Hz and 5 kHz when measured using an LCR Meter (TH2830, www.tonghui.com.cn). In contrast, the AC resistance of the Magstim D70 coil increased by up to 200% between 100 Hz and 5 kHz (Figs. 2j and S2g, h). Because of the significant reduction in coil current due to the magnetic core as well as the wearable design, only a 1.5-meter-long 10AWG (6 mm^2) connecting cable is required to meet the application requirements. Consequently, the total weight of the coil is controlled at 1.7 kg, equivalent to the weight of the Magstim D70 coil (1.76 kg) and meets the requirements for wearable applications.

Thanks to higher coil energy efficiency, the T2-Bent-D63 coil only requires a capacitance of 55 μF, whereas the Magstim D70 coil requires as much as 185 μF of energy storage capacitance at the same maximum voltage. This reduces the required volume of the energy storage capacitor to 30%, laying the foundation for wearable applications. The measured inductance of the T2-Bent-D63 coil can reach 57 μH, while the measured inductance of the Magstim D70 coil is 16 μH (Figs. 2k and S2i). Ignoring resistance, the oscillation angular frequency for biphasic TMS is $\omega = \sqrt{1/LC}$. Under 100% MSO (1600 V, 55 μF), we found that the T2-Bent-D63 coil's current waveform approximated a sine function. The maximum current was 1750 A, and the pulse width was 348 μs, with no apparent saturation of the magnetic core. In contrast, the Magstim D70 coil's maximum current was 5470 A (1670 V, 185 μF), and the pulse width was 342 μs (Fig. 2l). The T2-Bent-D63 coil's maximum current was only 32% of the Magstim D70 coil's current. Calculating using the formula for resistance losses, $P = I^2R$, under the same coil resistance (R) condition, the losses in power were reduced to approximately 10% of those of the Magstim D70 coil. The maximum dI/dt of rTMS-tiny was 31.6×10^6 A/s, which was 32% of that of the Magstim system. However, because of the bent-iron-core design, the rTMS-tiny induces a comparable electric field strength in the gray matter. More detailed information about the T2-Bent-D63 coil can be found in Table S2.

https://doi.org/10.1038/s41467-025-58095-9

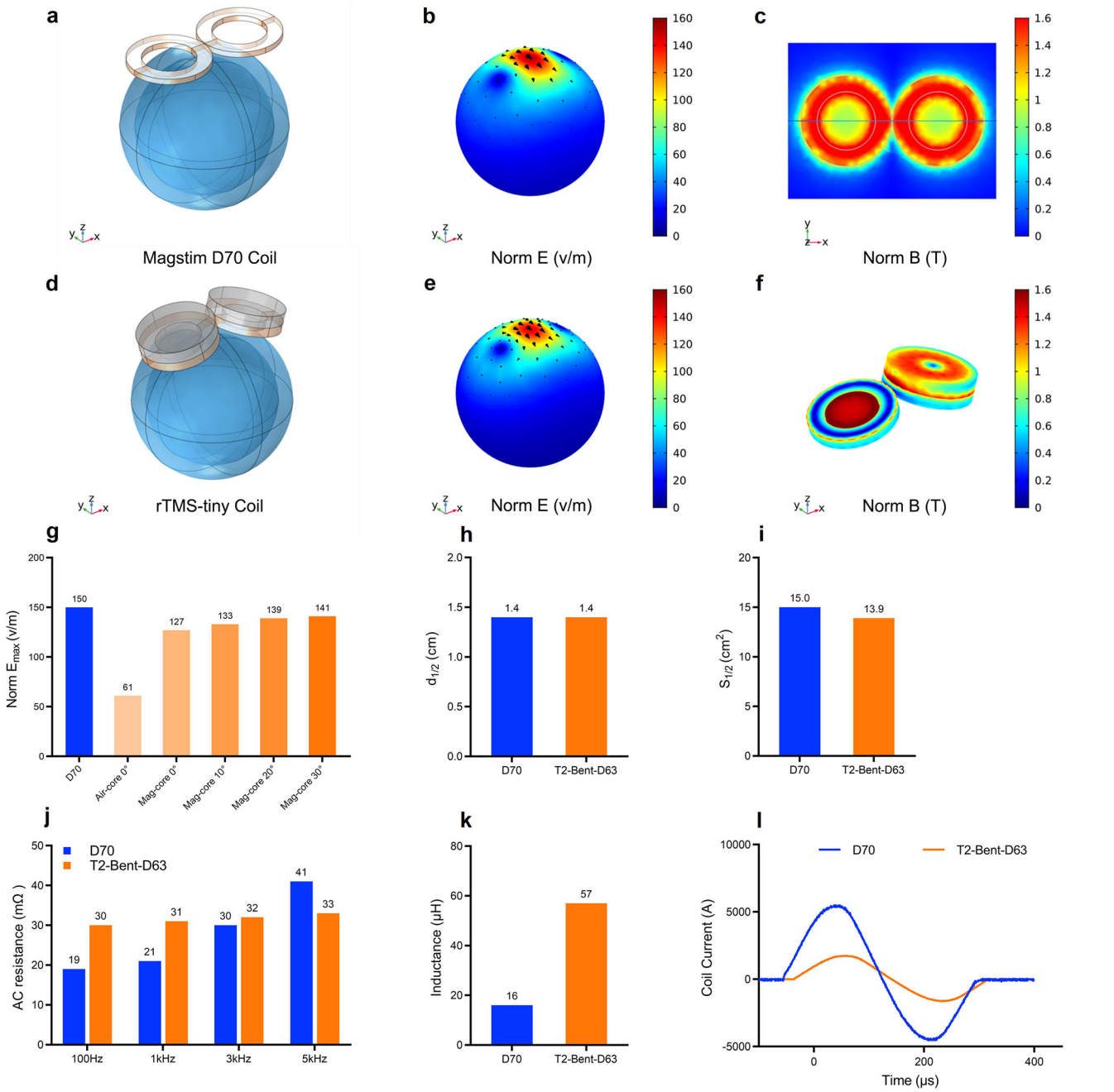

Fig. 2 | Coil design and performance. a–c Simulation of the Magstim D70 coil. **a** The coil is placed on a head model with a diameter of 85 mm and with gray matter located 15 mm beneath the scalp. The coil's surface is 5 mm from the scalp, representing the thickness of the coil's shell. **b** The electric field induced by the coil in the gray matter layer. **c** Distribution of the norm of B in the plane where the copper coil is located. **d–f** Simulation of the T2-Bent-D63 magnetic core coil. **d** T2-Bent-D63 placed on the same head model with the coil's surface 5 mm from the scalp. **e** The electric field induced by the coil in the gray matter layer. **f** Distribution of the norm of B in the magnetic core. **g** Maximum electric field intensity in the gray matter layer at 100% intensity. D70 represents the Magstim D70 coil, air-core 0° represents the T2-Bent-D63 without a magnetic core and bending, and mag-core 0°, 10°, 20°, and 30° represent T2-Bent-D63 with magnetic core bent angles of 0°, 10°, 20°, and 30°, respectively. **h** Comparison of half-value penetration depths $d_{1/2}$, the deeper the better. **i** Comparison of focalities, the smaller the better. **j** Comparison of coil AC resistance at different frequencies. **k** Coil inductance. **l** Measured waveform of coil currents.

Battery-powered, super-compact magnetic stimulator enables high-frequency repetitive pulse output

Due to the reduced coil current and capacitance capacity achieved by the T2-Bent-D63 magnetic core coil, it became feasible to create a lightweight and compact magnetic stimulator powered by batteries. We employed high-power-density, high-voltage pulse drive technology to realize the ultra-compact rTMS-tiny stimulator, weighing only 1.3 kg. This stimulator utilizes biphasic pulse output and efficiently recovers most of the energy in the coil to reduce losses and increase the repetition rate[38]. The circuit framework of the rTMS-tiny stimulator is shown in Fig. 3a, with the internal component structure illustrated in Fig. 3b. A 1600 V low-impedance, thin-film energy storage capacitor (2× SHB-800-110-4GB0, EACO) with a capacity of 55 μF is discharged instantaneously via an SCR (silicon-controlled rectifier) + a diode module (MCD94-22 IO1B, IXYS). The SCR trigger utilizes a pulse transformer for high-voltage isolation and triggering, with a trigger pulse voltage of 6 V, a maximum trigger current of 500 mA, and a pulse width of 100 μs. An RC snubber absorbs voltage

https://doi.org/10.1038/s41467-025-58095-9

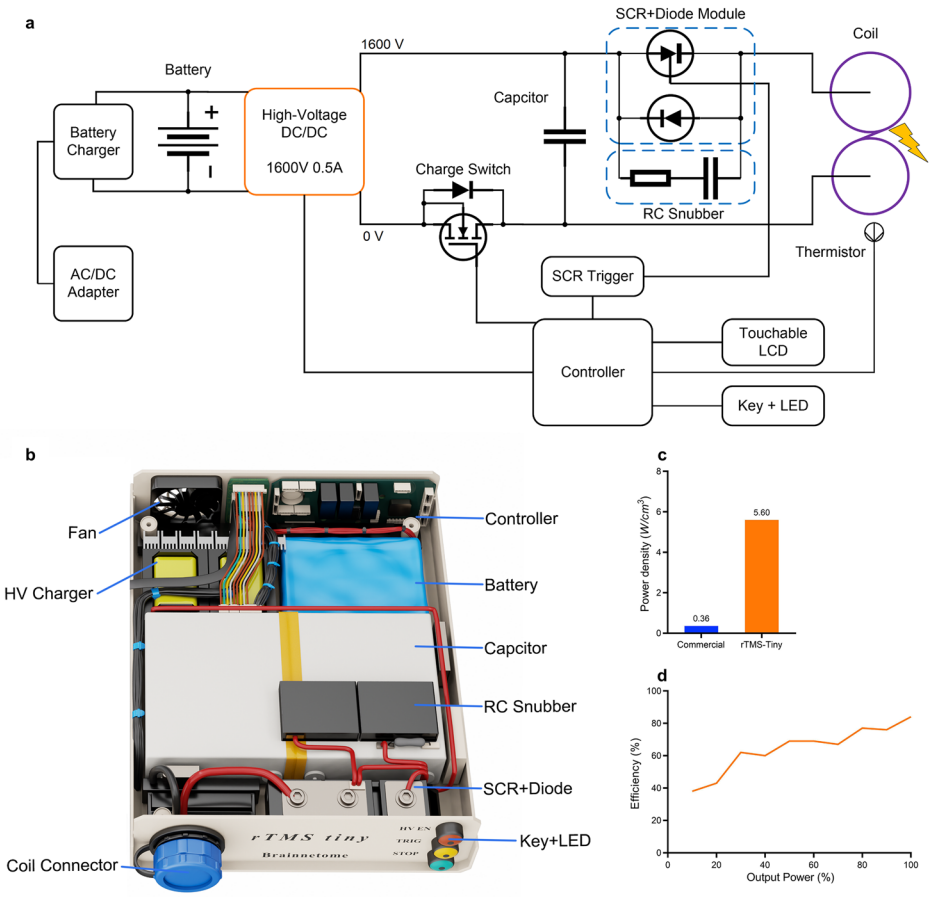

Fig. 3 | Principles and composition of the magnetic stimulator. a Schematic diagram of the rTMS-tiny magnetic stimulator's operating principles. **b** Internal structure of the rTMS-tiny magnetic stimulator. **c** High-voltage DC/DC power density in rTMS-tiny. The high-voltage DC/DC unit in rTMS-tiny boasts an impressive power density of up to 5.6 W/cm^3, significantly surpassing commercially available modules. This high level of power density is essential for achieving a highly portable and repetitive TMS pulse output. **d** Efficiency curve of rTMS-tiny's high-voltage DC/DC module. This demonstrates that the device maintains high efficiency across the entire output intensity range of 0–100% (0–1600 V).

overshoot during the SCR module's turn-off and reduces dv/dt to prevent damage or false triggering. After each magnetic pulse output, the energy storage capacitor is recharged by the high-voltage DC/DC module.

The output power of the high-voltage DC/DC module determines the repetition rate. In a previous study[23], a 1000 V, 30 mA high-voltage DC/DC module was used to charge a 1200 μF capacitor, taking 45 s to fully charge. In another study[39], a 10 W high-voltage DC/DC module required 23 s to charge the capacitor. Abbasi et al. used a driving circuit weighing 2.26 kg, along with a small (38 mm diameter), lightweight (12.6 g) figure-8 coil, to achieve 10 Hz rTMS with an electric field of 87 V/m at a depth of 1.5 cm. The system was equipped with a battery-powered 350 V boost converter[26,27]. In summary, existing high-voltage DC/DC modules provide insufficient output power, making wearable supra-threshold rTMS unfeasible.

We developed a high-power-density, high-voltage DC/DC converter module using multiple transformers in series and a voltage-doubling rectification technique. The block diagram of the high-voltage DC/DC converter is shown in Fig. S4a. In addition to the traditional "PWM controller" and "full-bridge MOSFET" components, "multi-transformers in series" and "full-wave voltage doubler" were employed to achieve higher efficiency. In the multi-transformers in series design, the primary windings are connected in parallel, and the secondary windings are connected in series, which increases the voltage boost ratio. The full-wave voltage doubler rectifier provides an additional 2× voltage boost while also eliminating the need for large inductance, as compared with the full-wave rectifier design (Fig. S4b). This approach reduces the number of windings and the distributed capacitance in individual transformers, increases the switching frequency, and thus significantly enhances the power density. With a compact form factor of 6 cm × 6 cm × 4 cm and a weight of 160 g, our rTMS device provides an output capacity of 1600 V and 500 mA, with a maximum output power of 800 W. The power density reaches 5.6 W/cm^3, and the 55 μF capacitor voltage rise rate is 9000 V/s. The voltage output range is 0–1600 V, and it has a high efficiency across the entire voltage output range, achieving a maximum efficiency of 84% (Fig. 3d). In contrast, commercially available high-voltage DC/DC modules, such as HO1-P202-20D (www.mornsun-power.com), have a volume of 7.2 cm × 5.5 cm × 2.8 cm and can only output 2000 V and 20 mA, with a maximum power of 40 W and a power density of only 0.36 W/cm^3–15 times lower than our design (Fig. 3c).

Because the energy storage capacitor generates transient reverse high voltage during discharge, it is necessary to disconnect the path to the high-voltage DC/DC through the charging switch to prevent damage. The high pulse frequency of rTMS demands high-speed switching, which cannot be achieved with mechanical switches. Additionally, using resistors[23] to block reverse high voltage during the capacitor charging phase results in significant energy loss and heat generation. Therefore, a 3300 V breakdown voltage SiC MOSFET (G2R1000MT33J, GeneSic Semiconductor) is employed as the switch. Its on-state resistance is only 1 ohm, significantly reducing losses and heat generation.

https://doi.org/10.1038/s41467-025-58095-9

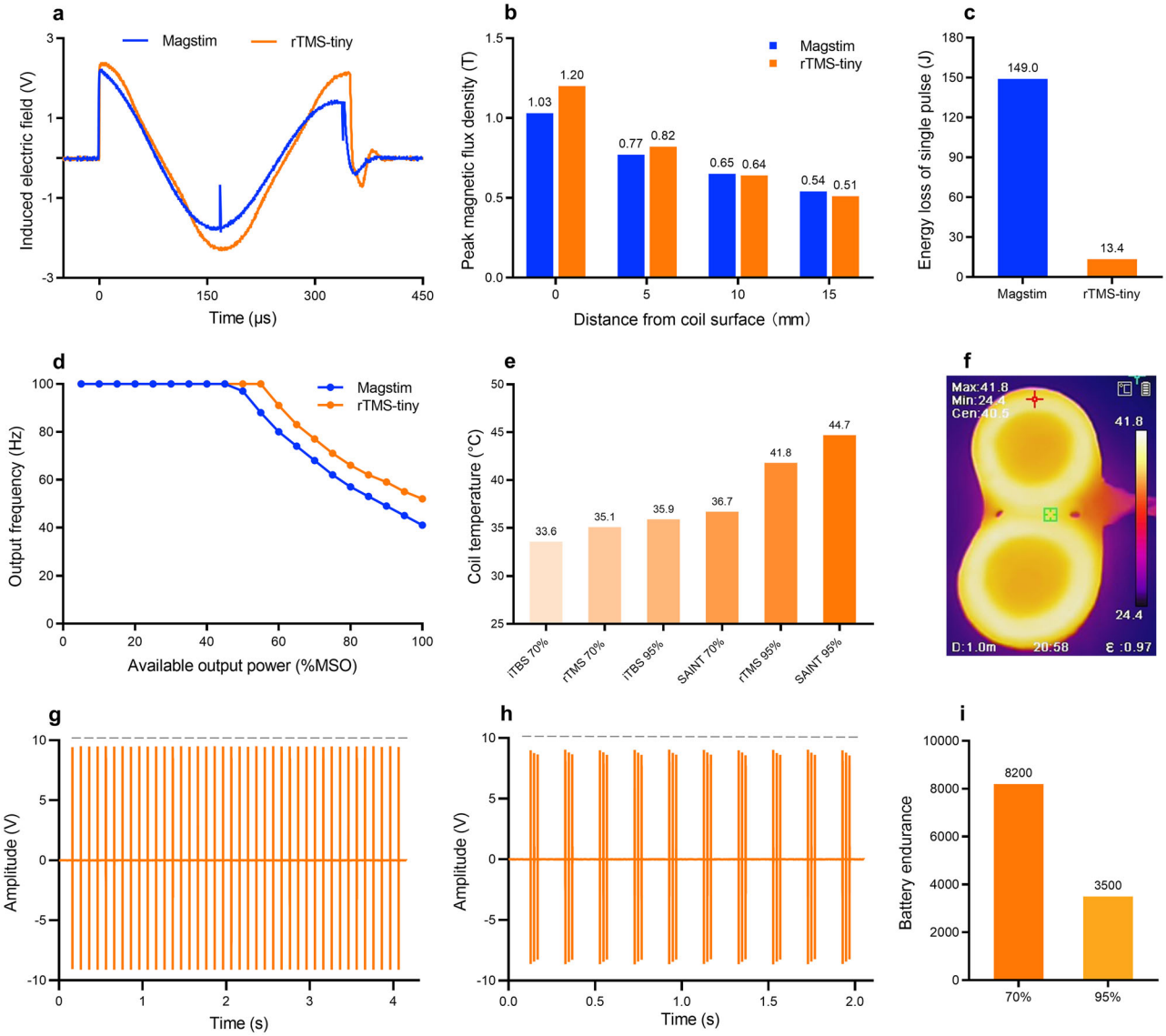

Fig. 4 | Overall performance testing. a Measured induced voltage waveform at the coil surface. **b** Peak magnetic flux density at different distances from the coil surface. **c** Single-pulse energy loss at 100% power. Magstim lost 149 J per single pulse, while rTMS-tiny lost only 13.4 J. **d** Relationship between the output frequency and the maximum available stimulus intensity. The stimulus intensity can reach 100% MSO for frequencies ranging from 1 Hz to 55 Hz. For frequencies greater than 55 Hz, the available stimulus intensity decreases. For instance, at 100 Hz, it decreases to 55% MSO. rTMS-tiny's repetitive output capability reached the level of the Magstim Super Rapid2 Plus conventional TMS device. **e** Coil temperature after stimulation given a starting temperature of 25 °C. Coil temperature remained within the requirements of IEC 60601-1. **f** Infrared thermal imaging of the coil after 3000 pulses of 10 Hz rTMS at 95% MSO. The heat diffused from the copper coil to the surroundings, with a maximum temperature of 41.8 °C. **g** rTMS waveform at 100% MSO. Pulse stimulation frequency is 10 Hz. No decay of stimulation intensity between pulses. **h** TBS waveform at 100% MSO. Pulse stimulation frequency is 50 Hz, 3 pulses form a cluster, with a repetition frequency of clusters at 5 Hz. Less than 5% decay of stimulation intensity within each cluster, and no decay of stimulation intensity between clusters. **i** Battery endurance. At 70% MSO, rTMS-tiny delivered 8200 pulses of 10 Hz rTMS, and at 95% intensity, it delivered 3500 pulses.

The rTMS-tiny magnetic stimulator's low power consumption, high efficiency, and ultra-compact design only require a 4 cm × 4 cm × 0.7 cm fan to meet the cooling needs. As a result, a stimulator weighing only 1.3 kg with a repetition rate of up to 100 Hz has been achieved.

Performance testing of the entire rTMS-tiny system

We conducted performance tests on the rTMS-tiny system and compared it with the Magstim's Super Rapid^2 Plus conventional TMS system. Both rTMS-tiny and Magstim had similar pulse widths, with rTMS-tiny having a pulse width of 348 μs and Magstim having a pulse width of 342 μs (Fig. 4a). The initial pulse amplitudes for both devices were also quite similar. The maximum magnetic flux density on the surface of the rTMS-tiny coil was 1.2 Tesla, which is greater than the Magstim D70 coil at 1.0 Tesla (Fig. S5d). As the distance from the coil surface increased, the magnetic flux density decayed, and the magnetic flux density of the two coils was almost the same (Fig. 4b). The electric field intensities were measured at different distances. The measurement setup is shown in Fig. S5e, following the method described by Abbasi et al.[26] and the results are shown in Fig. S5f and Table S3. These indicated that rTMS-tiny had an electric field intensity that is comparable to that obtained using Magstim.

In biphasic pulse TMS, some energy is returned to the energy storage capacitor after the discharge. The induced electric field is proportional to the coil voltage and, in the absence of SCR module and resistor voltage drops, also proportional to the energy storage

capacitor voltage. Therefore, the single-cycle decay of the induced electric field can be used to calculate the loss of capacitor energy. As seen in Fig. 4a, rTMS-tiny exhibited significantly lower single-cycle amplitude decay, with the capacitor voltage returning to 90% of the initial value, while Magstim's capacitor voltage only returned to 65%. Magstim has a capacitor capacity of 185 μF and a maximum voltage of 1670 V, whereas rTMS-tiny has a capacitor capacity of 55 μF and a maximum voltage of 1600 V. Through energy calculations ($E = 0.5CU^2$), we determined that at 100% MSO Magstim's initial energy is 258 J and decreases to 109 J after discharge, resulting in a single-pulse loss of 149 J. In contrast, rTMS-tiny's initial capacitor energy is 70.4 J and decreases to 57 J after discharge, resulting in a loss of only 13.4 J, which is less than 10% of Magstim's energy loss (Fig. 4c). This substantial reduction in energy loss leads to high energy efficiency.

Benefiting from the significantly reduced single-pulse energy loss and supported by the high-voltage DC/DC unit capable of outputting 1600 V 0.5 A, rTMS-tiny can achieve output up to 55 Hz pulses at 100% MSO (with less than 5% attenuation) (Figs. 4d and S5b). This capability enables a wide range of treatment paradigms, from 10 Hz rTMS to 50 Hz iTBS, and accelerated iTBS therapies such as SAINT therapy[40]. For the 10 Hz rTMS application, rTMS-tiny's output power could be set to 100% MSO with no decay of stimulus intensity between pulses (Fig. 4g). For the 50 Hz TBS applications (3 pulses form a cluster with a repetition frequency of clusters at 5 Hz), rTMS-tiny's output power could also be set to 100% MSO with less than 5% decay of stimulus intensity within each cluster and no decay of stimulus intensity between clusters (Fig. 4h).

Under the natural cooling of room temperature, 25 °C, the coil temperature was measured after 3000 pulses of 10 Hz rTMS, 600 pulses of iTBS, and 1800 pulses of SAINT treatment at both 70% MSO and 95% MSO. Except for the 95% MSO SAINT treatment, which reached a maximum coil temperature of 44.7 °C, the coil temperature did not exceed the maximum temperature of 43 °C allowed for prolonged human contact according to IEC 60601-1 standards (Fig. 4e). In addition, SAINT therapy is applied for a very short time, less than 10 min, and thus also complies with the 48 °C upper-temperature limit allowed by IEC 60601-1 for less than 10 min.

Heating remains a significant limitation for wearable rTMS systems, prompting additional tests and analyses. The surface temperatures of the coils were measured after each train using an infrared thermal imager (Fig. S6c–e) until the temperature reached 40 °C. The temperature curves for three types of coils (Magstim D70, D70 AFC, and rTMS-tiny) at two stimulation intensities (95% MSO and 70% MSO) are shown in Fig. S6a. The Magstim D70 coil overheated after 400 pulses at 95% MSO or 600 pulses at 70% MSO, with the surface temperature reaching up to 70 °C. In contrast, the rTMS-tiny and D70 AFC coils exhibited similar increasing temperature patterns and could sustain up to 3000 pulses without overheating.

Next, differences in heating between rTMS-tiny coil and the Magstim D70 coil were compared using the maximum number of trains as the dependent variable, to compute a two-factor ANOVA with the factors being the power levels (70% MSO and 95% MSO) and each coil type, as illustrated in Fig. S6b. The statistical analysis revealed significant differences in pulse counts between the coils (F (1, 9) = 1932.978, $p < 0.001$), between the two intensities (F (1, 9) = 12.490, $p = 0.006$), and in their interaction (F (1, 9) = 8.804, $p = 0.016$).

Additionally, the internal temperature of the rTMS-tiny stimulator was measured immediately after 3000 pulses at 95% MSO (Fig. S6f). The maximum temperature of the high-voltage DC/DC module reached 62.4 °C, and the maximum temperature of the battery was 48 °C. These temperatures were within acceptable limits. Temperature sensors were installed on both the DC/DC module and the battery so that, in the event of abnormal temperature readings, the rTMS-tiny would trigger an alarm and halt the stimulation immediately.

rTMS-tiny is powered by an 18 V 2200 mAh lithium battery. Under battery power, rTMS-tiny can deliver 8200 pulses at 70% MSO for 10 Hz of rTMS, supporting at least 2 standard rTMS treatments or 10 iTBS treatments. At 95% MSO, it can deliver 3500 pulses, supporting at least 1 standard rTMS treatment or 5 iTBS treatments (Fig. 4i). When an external 24 V 2.5 A power adapter is connected, continuous operation is supported.

Stimulus intensity testing on humans

Motor-evoked potentials (MEPs) in the peripheral muscles, obtained by stimulating the human motor cortex using TMS, is a non-invasive quantitative marker of cortical and spinal excitability[41]. MEPs also serve as a quantitative basis for calibrating individual TMS intensities[42]. To validate the stimulus intensity of the rTMS-tiny on humans, we conducted a comparative study of stimulus intensities between rTMS-tiny using T2-Bent-D63 coil and Magstim using D70 coil on humans. The participants were fifteen young, healthy volunteers, 9 males and 6 females aged 25 to 40 years, all right-handed. The study was approved by the Ethics Committee of the Institute of Automation, Chinese Academy of Sciences and we have obtained informed consent from all participants. Each participant underwent experiments on the abductor pollicis brevis (APB) muscles of both hands (Fig. S7) and the tibialis anterior (TA) muscles of both legs (Fig. S8), in the sequence of right hand, left hand, right leg, and left leg. The order of trials with Magstim and rTMS-tiny alternated between the participants to minimize any potential effects of neuroplasticity.

Figure 5a and Table S4 show resting motor threshold (RMT) values for the bilateral hands and legs. No significant differences were observed in the RMT values obtained with Magstim and rTMS-tiny for the left ($t(45.00) = 1.257$, $p = 0.621$; $RMT_{Magstim} = 79.8\%$, $RMT_{rTMS\text{-}tiny} = 82.6\%$) and right ($t(45.00) = 2.434$, $p = 0.073$; $RMT_{Magstim} = 81.9\%$, $RMT_{rTMS\text{-}tiny} = 87.2\%$) legs. Even though rTMS-tiny had a significantly higher RMT value for left (t (45.00) = 3.431, $p = 0.005$; $RMT_{Magstim} = 68.2\%$, $RMT_{rTMS\text{-}tiny} = 74.6\%$) and right ($t$ (45.00) = 3.585, $p = 0.003$; $RMT_{Magstim} = 64.7\%$, $RMT_{rTMS\text{-}tiny} = 71.4\%$) hands. The ratio of rTMS-tiny's RMT to Magstim's RMT was 91.5% for the left hand, 90.6% for the right hand, 96.6% for the left leg, and 93.9% for the right leg. These results are consistent with the concept that, since the output power of both devices was linear, the maximum stimulus intensity of rTMS-tiny would exceed 90% of Magstim's.

Figure 5b, c and Table S5 show the MEP amplitudes for both hands and both legs at different output powers ranging from 50% to 100% MSO. Significant differences in MEP amplitudes were seen for the right hand across various intensities ($F(5, 70) = 35.248$, $p < 0.000$), between two coils ($F(1, 14) = 12.274$, $p = 0.004$), and their interaction ($F(5, 70) = 4.016$, $p = 0.012$). MEP amplitudes for the left hand showed significant differences across intensities ($F(5, 70) = 16.000$, $p < 0.000$), but not between two coils ($F(1, 14) = 2.997$, $p = 0.105$) or their interaction ($F(5, 70) = 0.628$, $p = .538$). The right leg's MEP amplitudes were significantly different between intensities ($F(5, 70) = 20.535$, $p < 0.000$) and between coils ($F(1, 14) = 7.186$, $p = 0.018$), but not when they interacted ($F(5, 70) = 4.183$, $p = 0.051$). The left leg's MEP amplitudes were significantly different between intensities ($F(5, 70) = 29.854$, $p < 0.000$), but not between two coils ($F(1, 14) = 1.600$, $p = 0.227$) or their interaction ($F(5, 70) = 2.487$, $p = 0.120$).

Comparing the mean MEP amplitudes induced by Magstim and rTMS-tiny at 80%, 90%, and 100% MSO in Fig. 5b, c and Table S5, we found that the MEP amplitudes elicited by rTMS-tiny's 100%MSO and Magstim's 90%MSO were roughly the same. This was consistent with our previous finding that rTMS-tiny's maximum stimulus intensity was around 90% of Magstim's. Figures S10 and S11 show a typical participant's MEP waveforms for the right hand and the left leg under different amounts of stimulator output power.

https://doi.org/10.1038/s41467-025-58095-9

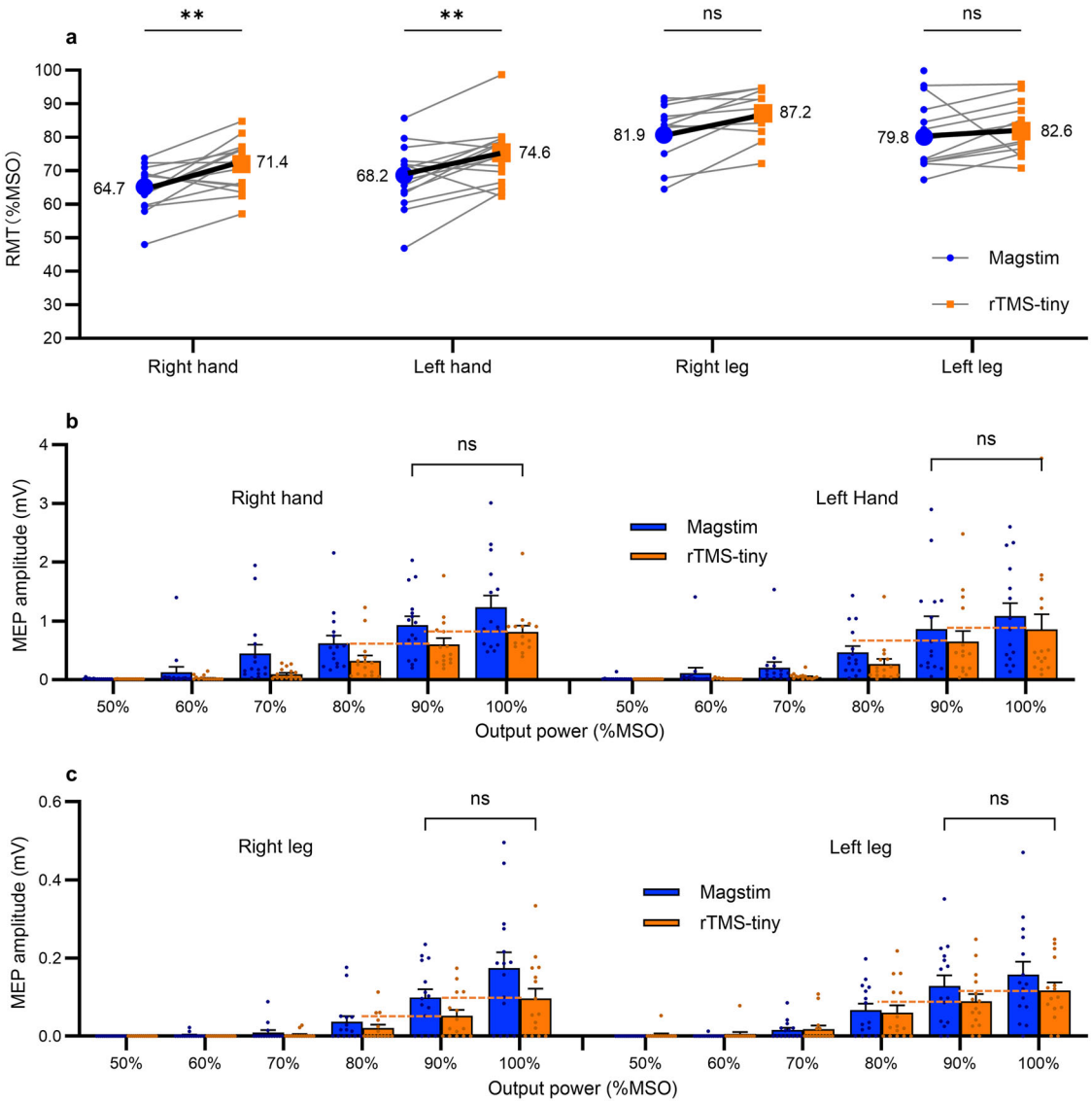

Fig. 5 | Stimulus intensity testing on humans. a RMT test results for both hands and both legs. The smaller dots denote each participant's RMT value. The larger dots denote the mean RMT values ($n = 15$). The mixed-effects analysis was used to analyse RMT values, and p values were 0.003, 0.005, 0.073, and 0.621, respectively. **b** MEP amplitudes for both hands APB muscles in 15 subjects under output power ranging from 50% to 100% MSO. Comparing the MEP amplitudes induced by Magstim and rTMS-tiny at 80%, 90%, and 100% MSO, showed that the maximum stimulus intensity of rTMS-tiny is about 89% of Magstim for the right-hand APB muscle and 90% for the left-hand APB muscle. c MEP amplitudes for both legs TA muscles in 15 subjects under output power ranging from 50% to 100% MSO. Comparing the MEP amplitudes induced by Magstim and rTMS-tiny at 80%, 90%, and 100% MSO showed that the maximum stimulus intensity of rTMS-tiny is about 90% of Magstim for both legs TA muscles. Error bars denote standard errors of the means. A total of 10 technical replicates were used to calculate the MEP amplitudes in (**a**–**c**). We did not establish the control group using a sham TMS coil because it is clear that no MEP or RMT can be elicited by the sham coil.

In summary, based on the average RMT values across all limbs, rTMS-tiny reached a maximum stimulus intensity of approximately 90–100% of Magstim's. Based on MEP amplitudes across all limbs, rTMS-tiny reached a maximum stimulus intensity of approximately 90% of Magstim's. Minor discrepancies may be attributed to data fluctuations or the slightly smaller focus of rTMS-tiny compared with Magstim.

rTMS neural modulation during free walking

Smooth coordination of limb movements is crucial for our daily lives and sports activities. In some cases, the contraction of muscles on one side of the body can lead to increased excitability in the primary motor cortex associated with the other side of the body. This phenomenon is known as the "remote effect[43,44]. Its neural mechanisms are typically examined by assessing the amplitudes of MEPs elicited by TMS. Many studies have observed remote effects in various contexts. For instance, muscle relaxation of the ankle dorsiflexors reduces the cortical spinal excitability of hand muscles on the same side[45] and activities like teeth clenching and the preparation and execution of ankle muscle contraction[46] enhance the excitability of the hand muscle area in the cerebral cortex. The effects during motor execution are greater than during motor preparation[46] and motor imagery[43,47]. These findings suggest that there are strong neural interactions behind the coordination of movements in different body parts. However, due to the limitations of traditional TMS systems, these studies have been conducted with participants in seated and still positions, lacking demonstrations in natural and freely moving conditions. The emergence of wearable rTMS can allow such research to be conducted.

Fifteen right-handed participants aged between 25 and 40 years, with no history of neurological or psychiatric disorders, were recruited

for the study after obtaining informed consent from all participants. The study was approved by the Ethics Committee of the Institute of Automation, Chinese Academy of Sciences, and we have obtained informed consent from all participants.

First, the remote effect in seated states was demonstrated using both rTMS-tiny and Magstim's rTMS devices. The participants were asked to make a fist with their hands to activate the upper limbs (Fig. S12a) and were asked to perform a plantar flexion to activate the lower limbs (Fig. S12b). Significant increases in MEP amplitudes of the right-hand APB muscle were observed during plantar flexion of either leg ($F(3, 42) = 8.132$, $p = 0.003$) (Fig. S12c), but no significant effect was found for the left-hand APB muscle ($F(3, 42) = 0.214$, $p = 0.771$) (Fig. S12d) or for the left ($F(3, 36) = 2.514$, $p = 0.074$) or right ($F(3, 30) = 1.620$, $p = 0.206$) leg TA muscles (Fig. S12e, f).

Second, the remote effect during free walking was demonstrated using rTMS-tiny. The T2-Bent-D63 magnetic coil was securely fastened to the M1 hand motor area using an elastic band to ensure that the coil remained in close contact with the head and in a stable position. The accuracy of the coil position and orientation was not tested, and the stability of the coil location with the elastic band was not validated. The rTMS-tiny stimulator and wireless muscle electromyography (EMG) measurement equipment were carried on the back of the participants, with the EMG sensor attached to the APB muscle of the right hand. The wireless EMG measurement device transmitted the collected EMG data to a PC via Bluetooth (Figs. 6a and S17a). The experiment began with the participants in a still seated position, the hand motor hotspot was located, and the RMT was determined. Subsequently, while remaining in a still position, participants were stimulated at 120% RMT every 6 s for 10 MEP recordings. Following this, the participants slowly stood up, with their arms naturally hanging down, and continued walking freely, with another 10 MEP recordings taken in this state (Fig. 6b-d). A paired t-test revealed that the MEP amplitudes during free walking significantly increased by over 100% compared with the still state ($t = 4.349$, df = 14, $p < 0.001$; Figs. 6e and S14–16). An unpaired t-test showed that this enhancement was significantly greater than the increase observed during plantar flexion in the seated position ($t = 2.056$, df = 28, $p = .0492$; Fig. 6f). The ability to carry out rTMS on the motor cortex at different stimulation frequencies (5 Hz, 10 Hz, 50 Hz) during free walking was also demonstrated (Fig. S17b–d).

This study provided the first evidence of a remote effect during free walking, demonstrating the ability of the wearable rTMS to achieve stable neural modulation during free behaviors. This finding, as well as others that maybe identified in future experiments, may provide some clues for stroke rehabilitation.

Discussion

We developed a battery-powered wearable rTMS device with significantly lower power consumption and volume than commercial devices yet able to maintain comparable stimulus intensity and repeat frequency. We demonstrated that our wearable rTMS device's maximum stimulus intensity on humans was approximately 90% of a commercial rTMS device and successfully induced both hands and legs MEPs. This innovation facilitates high-frequency rTMS on-the-go, promoting convenient home and community treatments.

We demonstrated neural modulation with rTMS during free walking, showing that the neural activity of one limb muscle during free walking can impact the activity of other limb muscles. This highlights the stable neural modulation capabilities of wearable rTMS during certain free behaviors such as walking steadily. This finding opens new avenues for research in the field of stroke rehabilitation and addresses challenges in applying rTMS during motor rehabilitation training, possibly leading to enhanced therapeutic effects[48,49]. Wearable rTMS offers the potential to investigate the dynamic changes in brain function during natural scenarios and free behaviors, allowing for the disruption of specific brain regions through rTMS, subsequently influencing behavioral decisions and cognitive functions. This approach unveils the functional roles of different brain regions during various forms of free movement[50,51].

In the context of home and community applications, wearable rTMS has the potential to revolutionize the treatment of neuropsychiatric disorders. The rTMS treatment of neuropsychiatric disorders such as depression typically occurs within hospitals. This approach incurs high costs, requires trained medical professionals, and necessitates daily treatments over one month[5,17]. However, many patients need to maintain their regular work routines, making it challenging to adhere to daily hospital visits, resulting in high drop-out rates and significantly affecting treatment outcomes[18,19]. Wearable rTMS will allow patients to administer treatment at their convenience—whether at home, work, or while traveling—providing unprecedented convenience. It has the potential to significantly reduce the time burden on patients and ease the strain on hospitals and may enable the widespread adoption of rTMS therapy while unleashing its full potential.

Wearable rTMS may also enable researchers to conduct longitudinal studies and assess the long-term effects of neuromodulation over extended periods. Conventional TMS is typically used for shorter, controlled sessions in laboratory settings. The device that we present here can be integrated with brain-computer interfaces (BCIs) for real-time cognitive enhancement during everyday tasks[52]. When combined with brain recording and decoding techniques, TMS-tiny should be able to achieve closed-loop neuromodulation by incorporating adaptive algorithms to adjust stimulation parameters based on the user's real-time brain activity or cognitive state[53]. The wearable nature of TMS-tiny provides new possibilities for closed-loop neuromodulation, as certain brain activity or cognitive states may not be replicable in laboratory settings, where conventional TMS is typically used.

The development of wearable rTMS devices opens the door to new possibilities for home-based therapeutic applications. However, the transition from traditional clinical settings to wearable devices introduces unique challenges, particularly in ensuring both electrical and medical safety. For instance, the high voltage and current levels required for rTMS stimulation necessitate robust insulation and emergency fail-safes to prevent accidental exposure. Additionally, the risk of rTMS-induced seizures must be carefully managed through physician-controlled settings, initial supervised sessions[4], and patient education.

For the electrical safety, we have taken the following measures: **(1)** The 1.6 kV high voltage and 1.7 kA high current inside the rTMS-tiny's main body and coils are all protected by a high-strength insulated enclosure, and the connecting cables are also insulated with a double layer of high-strength insulation, so that the human body will not come into contact with the high voltage. **(2)** The high-voltage storage capacitor has a capacity of 55 μF and a maximum energy storage of 70 J. Even in the event of a serious failure, the energy is not enough to break through the mechanical protection of the insulated enclosure. **(3)** rTMS-tiny has an emergency stop button. Pressing the emergency stop button will immediately turn off the high-voltage DC/DC and release the energy stored in the capacitor at the same time. **(4)** rTMS-tiny is powered by battery, eliminating the risk of electric shock from AC power. The battery itself has a complete protection circuit, including overcharging, overcurrent, overheating, and preventing spontaneous combustion of the battery itself. The battery capacity is 2200 mAh, the nominal voltage is 18 V, and the total energy is about 40 Wh, which is less than that of a laptop computer (the battery capacity of the Mac Book Pro is 70 Wh).

For the medical safety, we have taken the following measures: **(1)** The patients are not allowed to change the stimulation parameters of the rTMS-tiny by themselves. These parameters, including pulse intensity, pulse frequency, and number of pulses, are set through software permission settings, and one device is bound to one patient

https://doi.org/10.1038/s41467-025-58095-9

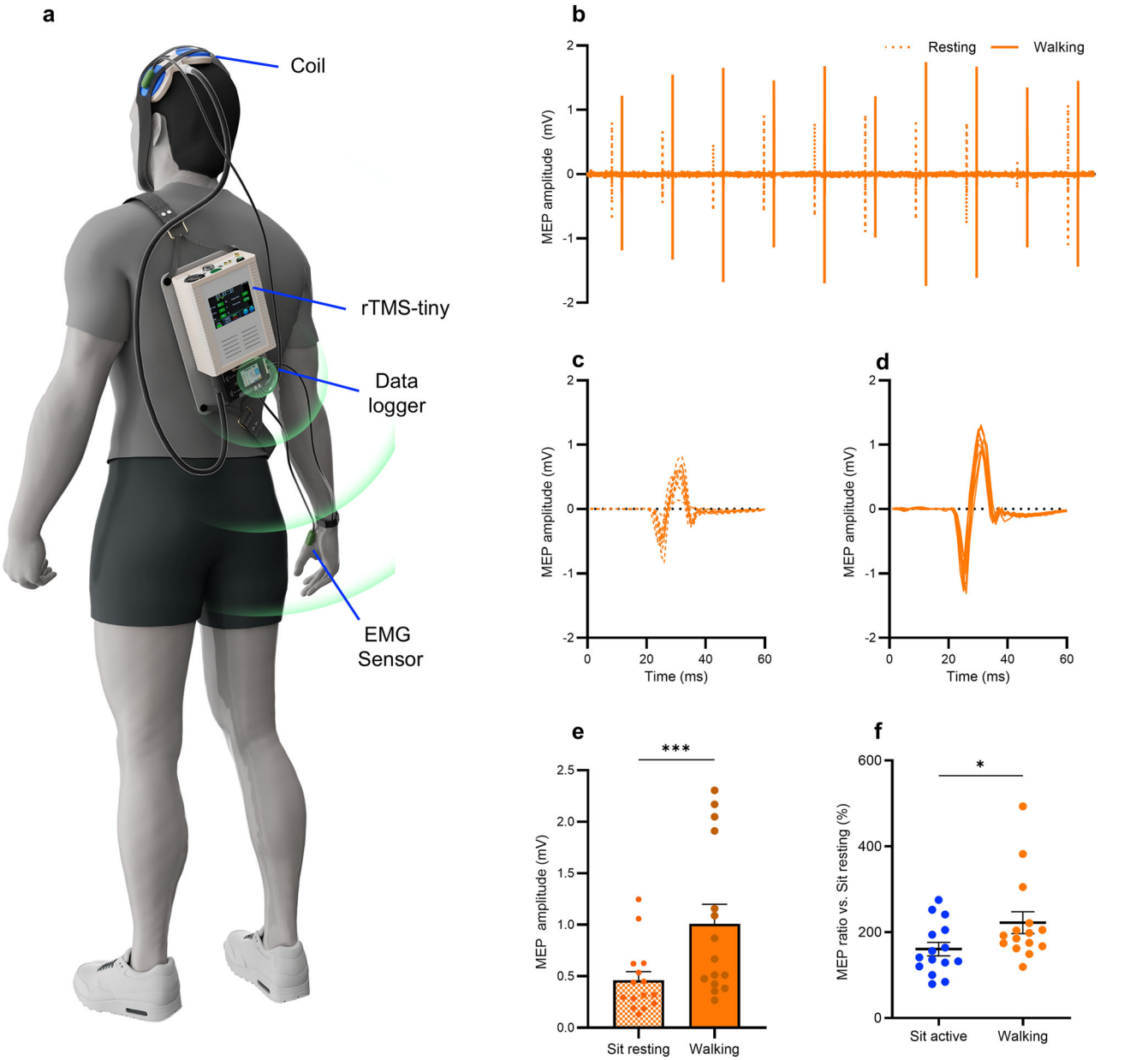

Fig. 6 | Neural modulation with rTMS during free walking. a The T2-Bent-D63 coil was securely fastened to the M1 hand motor area using an elastic band, ensuring that the coil remained in close contact with the head and in a stable position. The rTMS-tiny stimulator and wireless EMG measurement equipment were carried on the back. **b** Ten MEPs recordings were obtained at 120% of the RMT intensity in both the still and free walking conditions. **c** Typical MEP waveforms during resting. **d** Typical MEP waveforms during walking. **e** A two-tailed paired *t*-test statistical analysis of the MEP amplitudes from 15 participants demonstrated that the MEP amplitudes during free walking were significantly higher than those during the still state ($t = 4.349$, df = 14, $p < 0.001$). **f** The ratio of average MEP amplitude in 15 subjects between sitting with foot active and sitting resting, and between the walking and still states. The unpaired two-tailed *t*-test results from all participants consistently showed that the MEP amplitudes significantly increased during free walking and when sitting with the foot active ($t = 2.056$, df = 28, $p = 0.0492$). Error bars denote standard errors of the means. A total of 10 technical replicates were used to calculate the MEP amplitudes in (**e** and **f**). We did not establish the control group using a sham TMS coil because it is clear that no MEP can be elicited by the sham coil.

(via fingerprint, password, etc.), allowing only the physician to set it based on that patient's resting state motor threshold RMT, according to the latest IFCN rTMS safety guidelines[4]. **(2)** For patients without a history of epilepsy, the probability of seizures is extremely low when rTMS is modulated using the IFCN-recommended dosages, and the technology can largely be considered safe. Over 62% of seizures occurred on the first exposure to TMS, and 75% occurred within the first three exposures. Therefore, we will set the parameters in-hospital and perform the first treatment to expose seizure-prone patients, dramatically reducing the probability of developing seizures outside the hospital. **(3)** An adult with proper training must be present for rTMS treatment, and to avert emergency, we have incorporated a "one-button alarm" feature in the device's companion software, enabling patients to swiftly reach the local emergency medical service team via a single action.

The future success of wearable rTMS devices will depend on collaborative efforts between clinicians, engineers, and regulatory agencies to establish standardized protocols and ensure safe, effective, and user-friendly designs. These considerations underscore the importance of balancing technological innovation with rigorous safety precautions as we aim to make rTMS more accessible to diverse patient populations.

Methods

Coil electromagnetic field simulation

The simulation was conducted using COMSOL Multiphysics 5.4 with an AC/DC module. Since magnetic fields are minimally affected by the scalp, skull, cerebrospinal fluid, gray matter, or white matter, a simplified homogeneous water sphere model of the human brain was employed. This sphere had a diameter of 17 cm, with a 1.5 cm layer of gray matter beneath the scalp. The diameter of the gray matter region was 14 cm, and both regions were assigned an electrical conductivity of 0.33 S/m. The coil wire model was designed as a uniform multi-turn numerical coil, and the coil was excited using a current source. To account for the nonlinearity of the magnetic core and of possible magnetic core saturation, transient simulations were performed in COMSOL. The time range for each simulation was set to cover one TMS pulse width. The Magstim D70 coil's outer diameter was 87 mm, inner diameter 56 mm, and thickness 6 mm. Each side of the figure-8 coil had 9 turns. The coil was excited with a current of $5681 \times \sin(18372 \times t[1/s])$ [ampere]. The outer diameter of the T2-Bent-D63 coil was 78 mm, inner diameter 48 mm, and each coil had 14 turns. The excitation current was $1748 \times \sin(18055[1/s])$ [ampere], with both sides of the coil having the same current magnitude but opposite directions. Following previous research[36], the distance from the coils to the scalp was set to 5 mm to simulate coil insulation thickness and hair thickness. For the bending coil, the distance to the scalp was measured from the bottom of the perpendicular of the head sphere center to the coil's two lower planes, which is the minimum distance from the coil's lower surface to the head surface. The T-shaped magnetic core was constructed by connecting two thin cylinders: a small cylinder with a diameter of 4.6 cm and a height of 1 cm and a large cylinder with a diameter of 7.8 cm and a height of 1.3 cm. The magnetic core material selected was alloy powder HiFlux 125 mu.

Penetration depth and focality definition of the coil

Penetration depth $d_{1/2}$ refers to the depth of brain tissue where the induced electric field strength is greater than half the maximum induced electric field strength observed on the surface of gray matter (Fig. 2h). Focality is defined by $S_{1/2} = V_{1/2}/d_{1/2}$ where $V_{1/2}$ refers to the volume of brain tissue for which the induced electric field strength is greater than half of the maximum induced electric field strength observed on the surface of the gray matter[36] (Fig. 2i).

Magnetic coil manufacturing

The T2-Bent-D63 magnetic core is no longer a single continuous core but was transformed into two T-shaped cores in lateral projection. This configuration facilitates adjusting the angle and reduces weight. The T-shaped magnetic cores were manufactured by connecting a small and a large thin cylinder at their centers. The small cylinder had a diameter of 4.6 cm and a height of 1 cm, while the large cylinder had a diameter of 7.8 cm and a height of 1.3 cm. The core material employed was alloy powder HiFlux 125 mu, a high-saturation, low-loss, high-flux core made of 50% nickel and 50% iron with distributed air gaps, achieving a saturation magnetic flux density of up to 1.5 T, with an initial permeability (μr) of 125.

The coil winding was done using rectangular litz wire with a cross-sectional dimension of 2.1 mm × 5 mm. The litz wire consisted of 171 individual enameled wires with a diameter of 0.2 mm, resulting in an effective cross-sectional area of 5.37 mm^2. The filling factor was about 50%. The coil has 14 turns on each side, an inner diameter of 4.8 cm, an outer diameter of 7.8 cm, and a thickness of 1 cm. Each circular coil on either side was wound directly onto the T-shaped magnetic core in two layers, with 7 turns per layer. Subsequently, the two coils on either side were welded to form a figure-8 coil. A 1.5 m long 10 AWG (6 mm^2) connecting cable was soldered to the coils.

The coil and magnetic core were bonded and sealed using epoxy resin, forming a shell. Simple sealing molds were created using silicone gel. The curing process was accelerated by heating. Before complete curing, the coils were bent to the desired angle. At a thickness of approximately 2 mm from the coil to the shell surface, insulation strength and mechanical strength are ensured, reducing the distance between the coil and the scalp and enhancing stimulus intensity.

Power supply

The high-voltage DC/DC module is powered by a 5-series 20.8 V, 2200 mAh, 35 C high-rate lithium battery, capable of discharging more than 50 A and 1000 W. This design fulfills the power requirements of the high-voltage DC/DC module. The lithium battery is charged using a synchronous buck charging chip (MP2759) with a maximum charging current of 3 A and a charging efficiency of up to 96%. When the battery charge is insufficient, a 24 V, 2.5 A AC/DC power adapter (GSM60U, MEAN WELL) is used for charging, completing the process in approximately 1 h.

Controller

The controller is equipped with a 32-bit Cortex-M3 ARM MCU (STM32F103RCT, STMicroelectronics) operating at a frequency of 72 MHz. It boasts a rich set of resources, including ADC, DAC, timer, and more, to fulfill the rTMS control and human-machine interface requirements. The magnetic stimulator is equipped with a touchscreen display, enabling all human-machine interaction functions, including the stimulation mode and parameter configuration, information monitoring, and pulse triggering. It supports various operating modes, including sTMS, rTMS, and TBS. Additionally, the controller can real-time monitor the temperature of the coil, MOSFET, transformer, and battery by using multiple NTC thermistors (MF52-10K). It will automatically halt operation when temperatures exceed safe levels.

Pulse waveform and magnetic flux density measurement

A measuring coil with a diameter of 8 mm and 2 turns was wound with enameled wire with an outer diameter of 0.3 mm. The outlet of the measuring coil was tightly twisted to reduce magnetic field interference. These leads were then connected to an oscilloscope (DSOX3034T, KEYSIGHT). The measurement coil was placed horizontally in close proximity to the surface of the figure-8 coil (Fig. S3a). The TMS output power was set to 100%. When the TMS pulse output was triggered, the induced voltage pulse $E(t)$ was captured using an oscilloscope. The measurement coil's position was adjusted to find the location where the maximum induced voltage pulse was obtained, and this measurement was recorded and stored. The relationship between $E(t)$ and the magnetic flux intensity $B(t)$ is:

$$E(t) = \frac{dB(t) \cdot N \cdot S}{dt} \tag{1}$$

Where N is the measuring coil's turn number, and S is the measuring coil's area.

Integration of $E(t)$ yields the magnetic flux intensity waveform $B(t)$:

$$B(t) = \frac{1}{N \cdot S} \cdot \int E(t)dt \tag{2}$$

Coil temperature test

A coil temperature rise test (Fig. 4e, f) was conducted at room temperature (25 °C) to ensure that the coil does not become excessively hot and risk burning the skin. Temperature measurements were performed using a handheld thermal imaging camera, the H21Pro (www.hikmicrotech.com), with a measurement range of −20 °C to 350 °C and a nominal measurement error of less than ±2 °C. The H21Pro recorded the maximum temperature, and its measurement error in the range from 35 °C to 42 °C was determined to be less than +1 °C using a

thermometer with an error of ±0.1 °C. Prior to each test, the equipment was allowed to stabilize for at least 2 h at 25 °C to ensure that it reached room temperature. The coil temperature was measured immediately after conducting each of the following 6 stimulation protocols:10 Hz rTMS at 70% MSO, iTBS at 70% MSO, SAINT at 70% MSO, 10 Hz rTMS at 95% MSO, iTBS at 95% MSO, SAINT at 95% MSO. For the 10 Hz rTMS, each stimulation consisted of 4 s of stimulation followed by 26 s of rest, with a total duration of 37.5 min and 3000 pulses. The iTBS protocol consisted of bursts containing 3 pulses at 50 Hz repeated at 200 ms intervals, with 2 s of stimulation followed by 8 s of rest, totaling 600 pulses per session and a stimulation time of 3 min and 9 s. The SAINT therapy involved the continuous administration of iTBS for three sessions, totaling 1800 pulses.

EMG measurement and data processing

A wireless EMG measurement device, DataLog (Biometrics Ltd, USA), was used to collect the MEP data (Fig. 5a). The EMG sensors used were SX230 wired sensors with a noise level of less than 5 μV and a bandwidth of 20–460 Hz. A ground reference wristband was also employed to minimize interference. An additional EMG sensor was used to measure the induced voltage from the TMS coil as a marker to further eliminate interference and improve accuracy. This marker was more precise than digital markers. The method for creating the marker involved short-circuiting the two contacts of an EMG sensor using conductive copper foil. In the case of rTMS-tiny, the marker sensor was placed on the back of the magnetic core coil, while with the Magstim, the marker sensor was positioned on the coil handle to detect TMS pulse signals as markers. The sampling frequency was set to 1000 Hz. All collected data were processed using DataLINK PC Software Version 10.37. Each MEP was marked using the marker, and the statistical analysis was performed based on the peak-to-peak value of each MEP.

Comparison testing of MEP induction ability on humans

The participants were seated in a chair with their heads resting on a headrest to keep their heads still. A robotic neuro-navigation system (RC-M2N2-Duet, REALControl Co. Ltd., China) was used to hold the coil and perform precision TMS. First, the coil position was manually adjusted using a robotic arm to locate the motor hotspots. For the APB muscle, the coil was positioned on the left or right motor cortex with the coil handle angled at 45° to the midline pointing posteriorly (Fig. S4). For the TA muscle, the coil was placed 1–2 cm posterior to the vertex and 1–2 cm laterally to the left or right (Fig. S5). Individual adjustments were made to ensure maximal MEP amplitudes in the resting target muscles. Once the motor hotspots were identified, the robotic arm was fixed in place. Next, to determine the RMT more precisely and quickly, we employed an adaptive threshold estimation method instead of the '5-out-of-10 method[54,55]. In each search for an adaptive threshold, approximately 25–30 pulses were tested and the last 10 pulses were used to measure the resting-state MEPs at RMT (Fig. S6). Finally, the stimulus intensities were set at 50%, 60%, 70%, 80%, 90%, and 100% of the maximum stimulator output, and the MEP amplitudes were measured at each intensity level. The MEPs were automatically set to 0 if the stimulus intensity was below the RMT. The time interval between TMS pulses ranged randomly from 4 to 6 s to mitigate potential neuroplasticity effects. Figures S7 and S8 shows the typical participant's MEPs waveforms under different stimulator output powers. All the tracings had a smooth pre-trigger time window (100 ms), indicating that all the MEPs were recorded during full muscle relaxation. Each participant gave informed written consent.

Demonstration of remote effects while seated

All setups were identical to those used in the previous comparison testing of MEP induction ability on humans. Limb activation involved making a fist for the hands and plantar flexion for the legs (Fig. S9a). For the left-hand APB muscle, 10 resting MEPs at 120% RMT were first collected. Then, 10 MEPs at 120% RMT for each active state were collected in the following sequence: right hand active, right leg active, left leg active. For the right-hand APB muscle, the sequence was: resting, left hand active, left leg active, right leg active. For the left-leg TA muscle, the sequence was: resting, right leg active, right hand active, left hand active. For the right-leg TA muscle, the sequence was: resting, left leg active, left hand active, right hand active.

Statistics

We conducted a repeated ANOVA with intensity and coil type as factors to examine pulse counts during temperature elevation and MEP amplitudes elicited using TMS. To examine remote effects, we conducted an additional two-way repeated ANOVA to evaluate the MEPs induced by various types of TMS stimulators in the activation of different body parts. We used Mauchly's test to check for sphericity before all the analyses, and when needed, we also implemented a Greenhouse-Geisser correction. A Bonferroni correction was applied to post-hoc evaluations. All of our studies were carried out using Matlab 2024b (MathWorks, Natick, MA, USA). Furthermore, a mixed-effects analysis was conducted to evaluate the variation in RMTs assessed by different TMS coils.

Reporting summary

Further information on research design is available in the Nature Portfolio Reporting Summary linked to this article.

Data availability

All data are available in the supplementary materials, and in Figshare with the identifier https://doi.org/10.6084/m9.figshare.28089266.

Code availability

The codes used to compute the results and statistics, as well as generate visualizations are available in the supplementary materials, and in Figshare with the identifier https://doi.org/10.6084/m9.figshare.28089266.

References

1. Barker, A. T., Jalinous, R. & Freeston, I. L. Non-invasive magnetic stimulation of human motor cortex. *Lancet* **1**, 1106–1107 (1985).
2. Hallett, M. Transcranial magnetic stimulation and the human brain. *Nature* **406**, 147–150 (2000).
3. Merton, P. A. & Morton, H. B. Stimulation of the cerebral cortex in the intact human subject. *Nature* **285**, 227 (1980).
4. Rossi, S. et al. Safety and recommendations for TMS use in healthy subjects and patient populations, with updates on training, ethical and regulatory issues: expert guidelines. *Clin. Neurophysiol.* **132**, 269–306 (2021).
5. Pascual-Leone, A., Rubio, B., Pallardo, F. & Catala, M. D. Rapid-rate transcranial magnetic stimulation of left dorsolateral prefrontal cortex in drug-resistant depression. *Lancet* **348**, 233–237 (1996).
6. Lefaucheur, J. P. et al. Evidence-based guidelines on the therapeutic use of repetitive transcranial magnetic stimulation (rTMS): an update (2014-2018). *Clin. Neurophysiol.* **131**, 474–528 (2020).
7. Weise, K. et al. Precise motor mapping with transcranial magnetic stimulation. *Nat. Protoc.* **18**, 293–318 (2023).
8. Siddiqi, S. H., Kording, K. P., Parvizi, J. & Fox, M. D. Causal mapping of human brain function. *Nat. Rev. Neurosci.* **23**, 361–375 (2022).
9. Braun, P., Rapp, J., Hemmert, W. & Gleich, B. Coil efficiency for inductive peripheral nerve stimulation. *IEEE Trans. Neural Syst. Rehabil. Eng.* **30**, 2137–2145 (2022).
10. Koponen, L. M., Nieminen, J. O. & Ilmoniemi, R. J. Minimum-energy coils for transcranial magnetic stimulation: application to focal stimulation. *Brain Stimul.* **8**, 124–134 (2015).

11. Stangl, M., Maoz, S. L. & Suthana, N. Mobile cognition: imaging the human brain in the 'real world'. *Nat. Rev. Neurosci.* **24**, 347–362 (2023).
12. Hannah, R. & Aron, A. R. Towards real-world generalizability of a circuit for action-stopping. *Nat. Rev. Neurosci.* **22**, 538–552 (2021).
13. Boto, E. et al. Moving magnetoencephalography towards real-world applications with a wearable system. *Nature* **555**, 657–661 (2018).
14. Lang, C. et al. Complexities and challenges of translating intervention success to real world gait in people with Parkinson's disease. *Front. Neurol.* **15**, 1455692 (2024).
15. Di Pino, G. et al. Modulation of brain plasticity in stroke: a novel model for neurorehabilitation. *Nat. Rev. Neurol.* **10**, 597–608 (2014).
16. Harvey, R. L. et al. Randomized sham-controlled trial of navigated repetitive transcranial magnetic stimulation for motor recovery in stroke. *Stroke* **49**, 2138–2146 (2018).
17. O'Reardon, J. P. et al. Efficacy and safety of transcranial magnetic stimulation in the acute treatment of major depression: a multisite randomized controlled trial. *Biol. Psychiatry* **62**, 1208–1216 (2007).
18. George, M. S. et al. Daily left prefrontal transcranial magnetic stimulation therapy for major depressive disorder: a sham-controlled randomized trial. *Arch. Gen. Psychiatry* **67**, 507–516 (2010).
19. Wang, J. Mental health treatment dropout and its correlates in a general population sample. *Med. Care* **45**, 224–229 (2007).
20. Gutierrez-Muto, A. M. et al. The complex landscape of TMS devices: a brief overview. *PLoS ONE* **18**, e0292733 (2023).
21. Leung, V. et al. A Compact Battery-Powered rTMS Prototype. *2020 42nd Annual International Conference of the IEEE Engineering in Medicine & Biology Society (EMBC)* 3852–3855 (2020).
22. Moretti, J. & Rodger, J. A little goes a long way: neurobiological effects of low intensity rTMS and implications for mechanisms of rTMS. *Curr. Res. Neurobiol.* **3**, 100033 (2022).
23. Epstein, C. M. A six-pound battery-powered portable transcranial magnetic stimulator. *Brain Stimul.* **1**, 128–130 (2008).
24. Lipton, R. B. et al. Single-pulse transcranial magnetic stimulation for acute treatment of migraine with aura: a randomised, double-blind, parallel-group, sham-controlled trial. *Lancet Neurol.* **9**, 373–380 (2010).
25. Lee, S., Jang, K. I., Yoon, S. & Chae, J. H. The efficacy of miniaturized repetitive transcranial magnetic stimulation in patients with depression. *Clin. Psychopharmacol. Neurosci.***17**, 409–414 (2019).
26. Abbasi, S., Alluri, S., Leung, V., Asbeck, P. & Makale, M. T. Design and validation of miniaturized repetitive transcranial magnetic stimulation (rTMS) head coils. *Sensors.* **24**, 1584, (2024).
27. Leung, V. et al. A compact battery-powered rTMS prototype. *Annu. Int. Conf. IEEE Eng. Med. Biol. Soc.* **2020**, 3852–3855 (2020).
28. Koponen, L. M. & Peterchev, A. V. Transcranial magnetic stimulation: principles and applications. *Neural Engineering*. (ed. He, B.) 245–270 (Springer International Publishing, Cham, 2020).
29. Koponen, L. M., Nieminen, J. O., Mutanen, T. P., Stenroos, M. & Ilmoniemi, R. J. Coil optimisation for transcranial magnetic stimulation in realistic head geometry. *Brain Stimul.* **10**, 795–805 (2017).
30. Terao, Y. et al. Predominant activation of I1-waves from the leg motor area by transcranial magnetic stimulation. *Brain Res.* **859**, 137–146 (2000).
31. Deng, Z. D., Lisanby, S. H. & Peterchev, A. V. Coil design considerations for deep transcranial magnetic stimulation. *Clin. Neurophysiol.* **125**, 1202–1212 (2014).
32. Epstein, C. M. & Davey, K. R. Iron-core coils for transcranial magnetic stimulation. *J. Clin. Neurophysiol.* **19**, 376–381 (2002).
33. Barker, A. T. Stimulators and stimulating coils for magnetically stimulating neuro-muscular tissue Patent No. 6,663,556 (U.S. Patent and Trademark Office, Washington, DC, 2003).
34. Davey, K. & Riehl, M. Designing transcranial magnetic stimulation systems. *IEEE T Magn.* **41**, 1142–1148 (2005).
35. Yamamoto, K., Miyawaki, Y., Saitoh, Y. & Sekino, M. Improvement in efficiency of transcranial magnetic stimulator coil by combination of iron core plates laminated in different directions. *IEEE Trans. Magn.* **52**, 1–4 (2016).
36. Deng, Z. D., Lisanby, S. H. & Peterchev, A. V. Electric field depth-focality tradeoff in transcranial magnetic stimulation: simulation comparison of 50 coil designs. *Brain Stimul.* **6**, 1–13 (2013).
37. Gomez, L. J., Goetz, S. M. & Peterchev, A. V. Design of transcranial magnetic stimulation coils with optimal trade-off between depth, focality, and energy. *J. Neural Eng.* **15**, 046033 (2018).
38. Sommer, M. et al. Half sine, monophasic and biphasic transcranial magnetic stimulation of the human motor cortex. *Clin. Neurophysiol.* **117**, 838–844 (2006).
39. Charlet de Sauvage, R., Beuter, A., Lagroye, I. & Veyret, B. Design and construction of a portable transcranial magnetic stimulation (TMS) apparatus for migraine treatment. *J. Med. Devices* **4**, 015002 (2010).
40. Cole, E. J. et al. Stanford accelerated intelligent neuromodulation therapy for treatment-resistant depression. *Am. J. Psychiatry* **177**, 716–726 (2020).
41. Bestmann, S. & Krakauer, J. W. The uses and interpretations of the motor-evoked potential for understanding behaviour. *Exp. Brain Res.* **233**, 679–689 (2015).
42. Rossini, P. M. et al. Non-invasive electrical and magnetic stimulation of the brain, spinal cord, roots and peripheral nerves: basic principles and procedures for routine clinical and research application. An updated report from an I.F.C.N. Committee. *Clin. Neurophysiol.* **126**, 1071–1107 (2015).
43. Shironouchi, F. et al. Remote effects on corticospinal excitability during motor execution and motor imagery. *Neurosci. Lett.* **707**, 134284 (2019).
44. Delwaide, P. J. & Toulouse, P. Facilitation of monosynaptic reflexes by voluntary contraction of muscle in remote parts of the body. Mechanisms involved in the Jendrassik Manoeuvre. *Brain* **104**, 701–709 (1981).
45. Kato, K. et al. Muscle relaxation of the foot reduces corticospinal excitability of hand muscles and enhances intracortical inhibition. *Front Hum. Neurosci.* **10**, 218 (2016).
46. Komeilipoor, N. et al. Preparation and execution of teeth clenching and foot muscle contraction influence on corticospinal hand-muscle excitability. *Sci. Rep.* **7**, 41249 (2017).
47. Boroojerdi, B., Battaglia, F., Muellbacher, W. & Cohen, L. G. Voluntary teeth clenching facilitates human motor system excitability. *Clin. Neurophysiol.* **111**, 988–993 (2000).
48. Narayana, S. et al. Concurrent TMS to the primary motor cortex augments slow motor learning. *Neuroimage* **85**, 971–984 (2014).
49. Wang, Y. et al. Neural mechanism underlying task-specific enhancement of motor learning by concurrent transcranial direct current stimulation. *Neurosci. Bull.* **39**, 69–82 (2023).
50. Knoch, D., Pascual-Leone, A., Meyer, K., Treyer, V. & Fehr, E. Diminishing reciprocal fairness by disrupting the right prefrontal cortex. *Science* **314**, 829–832 (2006).
51. Figner, B. et al. Lateral prefrontal cortex and self-control in intertemporal choice. *Nat. Neurosci.* **13**, 538–539 (2010).
52. Luber, B. & Lisanby, S. H. Enhancement of human cognitive performance using transcranial magnetic stimulation (TMS). *Neuroimage* **85**, 961–970 (2014).
53. Tervo, A. E. et al. Closed-loop optimization of transcranial magnetic stimulation with electroencephalography feedback. *Brain Stimul.* **15**, 523–531 (2022).
54. Julkunen, P. Mobile application for adaptive threshold hunting in transcranial magnetic stimulation. *IEEE Trans. Neural Syst. Rehabil. Eng.* **27**, 1504–1510 (2019).

55. Wang, B., Peterchev, A. V. & Goetz, S. M. Three novel methods for determining motor threshold with transcranial magnetic stimulation outperform conventional procedures. *J. Neural Eng.* **20**, 056002 (2023).

Acknowledgements

The authors appreciate the English language and editing assistance of Rhoda E. and Edmund F. Perozzi, PhDs. Science and Technology Innovation 2030—Brain Science and Brain-Inspired Intelligence Project (Grant No. 2021ZD0200200, T.Z.J.); Natural Science Foundation of China (Grant No. 62327805, T.Z.J.); Key Collaborative Research Program of the Alliance of International Science Organizations (Grant No. ANSO-CR-KP-2022-10, T.Z.J.).

Author contributions

Conceptualization: Z.H.Q. and T.Z.J. Methodology: Z.H.Q. and T.Z.J. Formal analysis: Z.H.Q. and H.L. Investigation: Z.H.Q., H.L., X.F.L., and L.L. Visualization: Z.H.Q. Software: Y.H.W. and F.J. Funding acquisition: T.Z.J. Project administration: T.Z.J. Supervision: T.Z.J. Writing – original draft: Z.H.Q. and Z.Y.Y. Writing – review & editing: L.Z.F., M.S., N.M.Z., F.J., and T.Z.J.

Competing interests

The authors declare no competing interests.

Additional information

Supplementary information The online version contains supplementary material available at https://doi.org/10.1038/s41467-025-58095-9.

Correspondence and requests for materials should be addressed to Tianzi Jiang.

Peer review information *Nature Communications* thanks Vincent Leung, and the other, anonymous, reviewer(s) for their contribution to the peer review of this work. A peer review file is available.